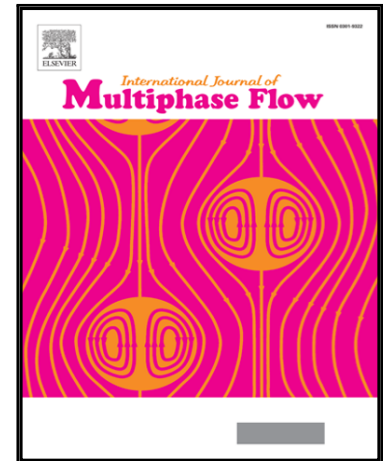


Accepted Manuscript

Local dissipation properties and collision dynamics in a sustained homogeneous turbulent suspension composed of finite size particles.

J.C.Brändle de Motta, J.L. Estivalezes, E. Climent, S. Vincent

PII: S0301-9322(16)30195-1
DOI: [10.1016/j.ijmultiphaseflow.2016.07.003](https://doi.org/10.1016/j.ijmultiphaseflow.2016.07.003)
Reference: IJMF 2434



To appear in: *International Journal of Multiphase Flow*

Received date: 4 April 2016
Revised date: 1 July 2016
Accepted date: 4 July 2016

Please cite this article as: J.C.Brändle de Motta, J.L. Estivalezes, E. Climent, S. Vincent, Local dissipation properties and collision dynamics in a sustained homogeneous turbulent suspension composed of finite size particles., *International Journal of Multiphase Flow* (2016), doi: [10.1016/j.ijmultiphaseflow.2016.07.003](https://doi.org/10.1016/j.ijmultiphaseflow.2016.07.003)

This is a PDF file of an unedited manuscript that has been accepted for publication. As a service to our customers we are providing this early version of the manuscript. The manuscript will undergo copyediting, typesetting, and review of the resulting proof before it is published in its final form. Please note that during the production process errors may be discovered which could affect the content, and all legal disclaimers that apply to the journal pertain.

LOCAL DISSIPATION PROPERTIES AND COLLISION DYNAMICS IN A SUSTAINED HOMOGENEOUS TURBULENT SUSPENSION COMPOSED OF FINITE SIZE PARTICLES.

J. C. BRÄNDLE DE MOTTA ^{1,2,3}, J. L. ESTIVALEZES ^{2,3}, E. CLIMENT ³, S. VINCENT ⁴

¹ *CORIA, Normandie Université, UMR CNRS 6614, Site Universitaire du Madrillet, 76801 Saint-Etienne du Rouvray, France*

² *ONERA, The French Aerospace Lab, 2, avenue Edouard Belin, 31055 Toulouse, France*

³ *Institut de Mécanique des Fluides de Toulouse (IMFT), Université de Toulouse, CNRS-INPT-UPS, Toulouse, France*

⁴ *Université Paris-Est Marne-la-Vallée, UMR CNRS 8208, Laboratoire MSNE, 5 boulevard Descartes, 77454 Marne-la-Vallée, France*

KEYWORDS : Particulate-flows, Turbulence, Finite-size particles, Local dissipation, Collision statistics

ABSTRACT. Particulate flows are present in many applications and the effect of particle size is still not well understood. The present paper describes three cases of sustained homogeneous turbulence interacting with particles. Simulations correspond to three particle-fluid density ratios and 3% volume fraction in zero gravity field. Fully resolved particle simulations are based on fictitious domain and penalty method.

The local dissipation around particles is studied according to the density ratio. Spatial description of the averaged dissipation is provided. Collision statistics are also investigated. The inter collision time and the angle of collision are compared to the kinetic theory. The effect of the inter particle film drainage is highlighted by simulating the same configurations with and without lubrication model.

E-mail address: jorge.brandle@coria.fr (corresponding author), estivalezes@onera.fr, climent@imft.fr, stephane.vincent@u-pem.fr.

CONTENTS

| | |
|--|----|
| 1. Introduction | 2 |
| 2. Simulation of finite size particles | 6 |
| 3. Macroscopic properties | 8 |
| 3.1. Energy distribution | 8 |
| 3.2. Particle statistics | 12 |
| 4. Dissipation distribution around particles | 14 |
| 4.1. Moving frame around particles | 14 |
| 4.2. Dissipation rate in a moving frame around particles | 16 |
| 5. Collision statistics | 20 |
| 5.1. Collisions with solid contact only | 20 |
| 5.2. The effect of lubrication on collision statistics | 26 |
| 6. Conclusion | 29 |
| References | 30 |

1. INTRODUCTION

Particle-laden flows can be found in natural environment and many industrial applications. For example, sediments in rivers, solid particles in fluidized beds, droplets in clouds or in combustion chambers [51] could be treated as particles. Depending on the regime, the turbulence can completely govern the particles' behaviour (spatial distribution, collision rate, ...). In the case of moderately concentrated to dense flows, the presence of particles can also influence the turbulence, [38, 5].

Dimensionless parameters characterising particle laden-flows are:

- the density ratio $\rho = \frac{\rho_p}{\rho_f}$, with ρ_p and ρ_f the density of the solid and fluid respectively,
- particle volume fraction,
- the Stokes number, defined as the ratio between the particle response time τ_p and a characteristic flow time scale τ_f . For the turbulent case, the Kolmogorov time scale is often chosen for τ_f . In this case the Stokes number is St_k . Nevertheless, this scale loses its relevance to predict finite size particle dynamics, *i.e.*, when the particle size is larger than the Kolmogorov length scale, [27].
- for finite-size particles, a new dimensionless parameter has to be considered, *i.e.* the ratio between the particle radius R and the Kolmogorov length scale η .

The motion of finite size particles in turbulent flow has received much less attention than small particles. Indeed, the size of the particles induces new coupling phenomena between fluid and particles, for example with flow scales larger than the Kolmogorov scales. In this case, classical Lagrangian pointwise approaches are not able to model these couplings as scale separation is not satisfied. Due to available CPU resources the computational cost of finite-size particle simulations was not affordable until recent years. More recently, with increasing power of massively parallel computers, the finite-size effect on particle dynamics has motivated many studies.

In figure 1, an extensive collection of relevant studies is presented. Experimental data, pointwise simulations and finite-size simulations are plotted together according to St_k , ρ and $\frac{R}{\eta}$. Studies are depicted with filled circles for simulations and open symbols for experiments. In addition, pointwise simulations have been reported as square symbols. It can be observed that pointwise simulations are focused on large density ratios, *i.e.* mostly gas/solid motions, whereas finite-size particle studies are concerned with Stokes numbers and density ratios ranging from 1 to 100. In order to contribute to the understanding of finite-size particle laden flows, fully-resolved turbulent simulations are considered in the present work for moderate density ratios corresponding to liquid/solid suspensions and St_k ranging from 10 to 100. These simulations are also reported in figure 1 (purple circles).

The main results obtained in the literature are now summarized:

- **Turbulence modulation**

The dispersed phase can modify the turbulent characteristics. This modulation can be split into three contributions. The first one is due to the force exerted by the particles on the fluid. For pointwise models, it can be written as the ensemble averaging $\langle \mathbf{u} \cdot \mathbf{f} \rangle$ obtained from the scalar product of the fluid velocity at the position of the particle \mathbf{u} and the force \mathbf{f} (see for example [16]). It was concluded that modulation depends on the Stokes number based on the Kolmogorov time scale. For different Stokes numbers, it was observed that point particles could enhance turbulence or dissipate energy. The second contribution is a transfer of energy from large to small scales, [16, 5]. Finally, a third contribution comes from the modification of local dissipation around the particles. This is typically a finite-size effect which cannot be accounted for by classical pointwise simulations.

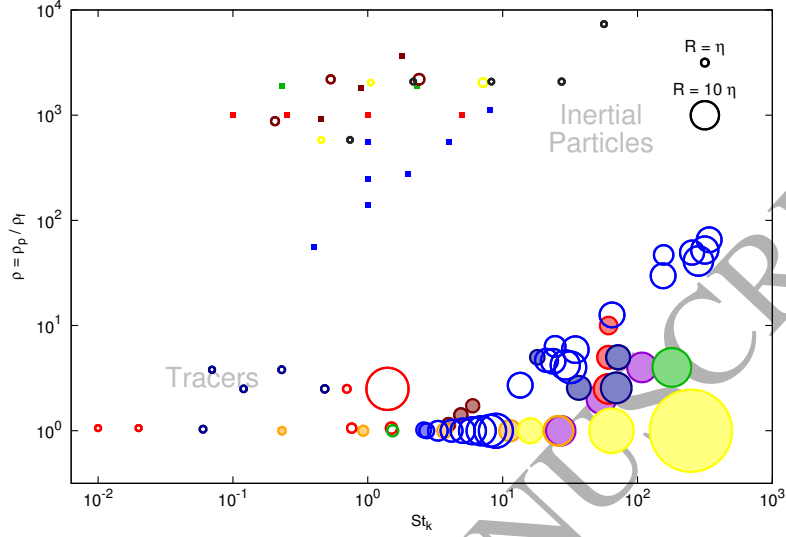


FIGURE 1. Representation of turbulent particulate flows according to the density ratio, Stokes number based on Kolmogorov scale and $\frac{R}{\eta}$ for finite size configurations. The square symbols represent the pointwise simulations (red: [16], green: [2], blue: [39], brown: [13]), the open symbols hold for experimental data (red: [50], green: [14], blue: [31], brown: [40], orange: [4], yellow: [49], dark blue: [30], black: [17]) and the filled circles correspond to the finite size particle simulations (red: [26], green: [11], blue: [52], brown: [42], orange: [20], yellow: [9], dark blue: [18] and [37], purple: present paper). The size of the circle is proportional to the ratio between the particles radii and the Kolmogorov length scale.

The effect of finite size particles on turbulence modulation was studied numerically in [52]. It is shown that the rate of decay of the turbulence is more important for the finite size case than for single-phase and particulate pointwise simulations. Actually, it is still necessary to understand and explain this effect. From the instantaneous dissipation fields obtained in the simulations of [42], it can be observed that a local dissipation appears around particles. Later, the study of [26] verifies that

the averaged dissipation increases around particles. In order to quantify this effect, the authors computed the averaged dissipation upstream and downstream of particles. The local increase of the dissipation is more important in the front and its spatial extension is about one diameter long. A similar conclusion is drawn in [9] in which a tentative explanation is given: the wake generated behind the particles decreases the turbulent dissipation level. These results are confirmed by the experiments of [40] concerning the study of dissipation around particles settling in a turbulent flow. The dissipation is multiplied by 3 in the front of the particles. The local dissipation will be analysed in the present paper.

The local dissipation is not the only finite size effect in turbulence modulation. In fact, as shown by [30], finite size particles can modify the turbulence structures without modifying the energy content. Finally, [26] shows that the coupling term $\langle \mathbf{u} \cdot \mathbf{f} \rangle$ is positive (energy enhancement) for finite size particles. For pointwise particles, this term generally dissipates energy.

- **Collision regime**

The study of the collision regime is important for many applications such as the prediction of coalescence rate of droplets. The collision rate represents the number of collisions per unit time. It can be obtained from the relative velocity of the particles $|w_r|$ and the radial distribution at contact g_0 , as follows,

$$(1) \quad f_c = \frac{1}{\tau_c} = \frac{1}{2} g_0 n_p^2 \pi (2R)^2 \langle |w_r| \rangle$$

where $\langle . \rangle$ is the ensemble average, τ_c is the collision time and n_p is the particle number density. The particle collision frequency in turbulent flow is relatively well described for two cases. In the first case, for particles with small response time (tracers), the collisions are driven by the local shear in the flow. The collision rate can be correlated to the dissipation rate of the flow, [36]. In the second case, where the particles are inertial, the Tchen-Hinze correlation [41, 19] links the particle kinetic energy to the turbulent statistics. Thus, the collision rate can be computed, [1]. For intermediate cases, many models have been proposed [48, 23, 24].

For finite size particles, only the study of [42] has addressed collision statistics. This study showed that secondary collisions

appear. The secondary collisions are consecutive collisions between pairs that stay correlated during a relatively long time. These collisions are not predicted by previous models. In the present paper, the secondary collision frequency will be analysed.

This article presents a study of a sustained homogeneous turbulent flow seeded with finite-size particles. First of all, the numerical method is summarized in section 2. The choice of the turbulent particle laden flow parameters is discussed in section 3. From this turbulent case, two major phenomena are studied. The first one is the averaged flow around particles which is described in section 4. The second phenomenon is the collisional regime detailed in section 5 where we focus on lubrication effects on collisional regime. Conclusions and perspectives are finally drawn in the last section.

2. SIMULATION OF FINITE SIZE PARTICLES

The modelling and simulation of fully resolved finite size particles in turbulent incompressible and isothermal fluid is investigated by means of a single fluid model [22] generalized for particulate flows [44]. The key idea is to use a fictitious domain approach in which an Eulerian description of the two-phase flow is introduced by a characteristic function C , also called volume of fluid (VOF). This function is 0 in the fluid phase and 1 in the solid phase. It allows to locate any point in a given phase by defining the interface as $C = 0.5$. The single fluid model is implemented on fixed structured Cartesian meshes not adapted to the shape of the fluid/particle interfaces, so that the particles are fictitious domains embedded in the calculation grid. The formulation of the single fluid model is the following (see [44] for more details)

$$(2) \quad \nabla \cdot \mathbf{u} = 0$$

$$(3) \quad \rho \left(\frac{\partial \mathbf{u}}{\partial t} + (\mathbf{u} \cdot \nabla) \mathbf{u} \right) = -\nabla p + \nabla \cdot (\mu (\nabla \mathbf{u} + \nabla^t \mathbf{u})) + \mathbf{f}_{si}$$

$$(4) \quad \frac{dC}{dt} = \frac{\partial C}{\partial t} + \mathbf{u} \cdot \nabla C = 0$$

where \mathbf{u} and p are the velocity field and the pressure respectively in both phases, t the time, ρ and μ the density and the viscosity of the equivalent fluid (fluid and solid phases). The density and the viscosity of the equivalent fluid are formulated according to the real physical

properties of the two different media and the VOF function by using arithmetic or harmonic weighting based on the local value of C . In order to enforce the solid body response of particles, the viscosity of the solid phase is 300 times the fluid one. Due to the Eulerian representation of the two-phase flow, a specific four way coupling term \mathbf{f}_{si} is added to the momentum equations in order to model collisions and lubrication. This force distribution results from a damp and spring collision representation and a lubrication model depending on the distance between interacting particles [6].

From a numerical point of view, the divergence free and solid constraints of the fictitious domain approach are approximated by finite volumes, an implicit viscous tensorial penalty method [34, 32] and an augmented Lagrangian minimization algorithm adapted for two-phase flows [45]. By using penalty methods and augmented Lagrangian techniques, the velocity, pressure and fluid/solid constraint are satisfied instantaneously and in a coupled manner at each time step. This way, the CFD code is robust and physically relevant. Concerning the advection equation (4) of the VOF function C , it is approximated in a Lagrangian manner in order to avoid deformation of the particle shape commonly observed in standard VOF methods [33]. In our approach, the center of mass of the particle is advected in a Lagrangian way with the velocity obtained thanks to mass and momentum balance equation (2-3). After this advection step, the analytical spherical shape of the particle is projected onto the Cartesian grid to update the C function. The final approximation of the global one fluid model for resolved scale particles converges spatially to second order.

The model and numerical methods have been widely validated on particle settling, Poiseuille and rotating flows, collisions and also on liquid/solid fluidized bed simulations in [34, 32, 6, 44].

A collision model is used to reproduce particle-particle interaction and rebound. During collisions, a force is exerted on the particle volume, \mathbf{f}_{si} . Two different forces are taken into account in order to model the effect of lubrication (fluid drainage) and the solid-solid collision force. These forces depend on the dimensionless gap between particle surfaces and on the normal relative velocity given by:

$$(5) \quad \epsilon = \frac{(\mathbf{X}_p^a - \mathbf{X}_p^b) \cdot \mathbf{n} - 2R}{R}, \quad u_n = \frac{(\mathbf{V}_p^a - \mathbf{V}_p^b) \cdot \mathbf{n}}{2},$$

where \mathbf{n} is the unit vector connecting the centers of the two particles. A detailed presentation of this model and validation against experiments are given in [6].

In order to compare the effect of lubrication model, each simulation presented in the following section has been carried out twice. A first simulation has been done with only the solid-solid collision model. A second one with both forces, solid-solid collision and lubrication.

The solid-solid collision is modelled by a spring and dash-pot force

$$(6) \quad F_s = -\frac{m_e (\pi^2 + [\ln(e_d)]^2)}{[N_c \Delta t]^2} R\epsilon - \frac{2m_e \ln(e_d)}{[N_c \Delta t]} u_n$$

where $m_e = (m_a^{-1} + m_b^{-1})^{-1}$ is the reduced mass, e_d is the dry restitution coefficient, defined as the ratio between the velocity after and before the collision, and $N_c \Delta t$ is the numerical collision time. In all simulations $e_d = 0.97$, thus the solid collisions are quasi-elastic. The number of fluid time steps for the solid numerical collision time N_c is fixed to 8. This force is activated at a distance ϵ_{ss} . This threshold is fixed to 0 for the simulations in which the lubrication force is activated and to 0.1 when this force is not taken into account. In order to compare similar collision with or without lubrication, ϵ_{ss} without lubrication has to be equal the threshold distance ϵ_{al} for lubrication.

The second force is a model of hydrodynamic interaction during the drainage of the liquid film between the particles. This hydrodynamic interaction is not captured directly by the numerical solution of the Navier-Stokes equations because the grid size is larger than the film thickness close to contact. The force is computed from the analytical expressions [7, 10],

$$(7) \quad F_l(\epsilon, u_n) = -6\pi\mu_f R u_n [\lambda(\epsilon) - \lambda(\epsilon_{al})]$$

$$(8) \quad \lambda = \frac{1}{2\epsilon} - \frac{9}{20} \ln(\epsilon) - \frac{3}{56} \epsilon \ln(\epsilon) + 1.346 + \mathcal{O}(\epsilon)$$

The lubrication force is activated for $\epsilon = \epsilon_{al} = 0.1$ which is equivalent to $0.6 \Delta x$. When the particles are near overlapping the force is kept constant. It has been shown that the addition of these two forces ensures the expected lubricated rebound in a viscous fluid [6].

3. MACROSCOPIC PROPERTIES

3.1. Energy distribution. Based on fully resolved simulations we aim at getting more insight on the collisional regime of finite size particles in a turbulent flow. In order to obtain converged collision statistics over long times, it is necessary to simulate sustained turbulence. To do so, turbulence is sustained by using the linear forcing proposed by [35].

In our implementation the velocity field \mathbf{u} is rescaled to \mathbf{u}^+ at each time step as to keep a constant kinetic energy fixed at the beginning of the simulation \mathbf{u}_0^2 within the simulation domain:

$$(9) \quad \mathbf{u}^+ = \sqrt{\frac{\int_{\Omega} \mathbf{u}_0^2 dv}{\int_{\Omega} \mathbf{u}^2 dv}} \mathbf{u}$$

The turbulence forcing is unsuitable for particle flow energy balance analysis [26]. In the present paper such detailed analysis is not provided. In addition the case considered is dilute, for this reason the two-way coupling effect remains negligible. We expect in the present paper that physics of the local dissipation and collision regime are not affected by the linear forcing.

A 256^3 mesh is used for direct numerical simulations enforcing adequate resolution of the Kolmogorov scale η (with $\eta/\Delta x = 0.56$). Simulating one large eddy turn-over time takes 10 h CPU on 512 cores of an SGI Altix Ice supercomputer.

In order to obtain the initial turbulent flow, a single-phase turbulence is initialized with a predefined homogeneous isotropic turbulence spectrum [28, 43]. Then, single-phase simulations with sustained turbulence are achieved with the previous forcing scheme until reaching steady state spectrum. The Taylor micro-scale Reynolds number of the turbulent flow computed from this spectrum is $Re_{\lambda} = 73$. This moderate Reynolds number corresponds to a moderate length scale separation: the ratio of Taylor micro-scale over Kolmogorov scale is $\lambda/\eta = 17$. First, the flow is forced from its initial condition (analytic spectrum) to reach statistical steady state. Then, 512 particles are seeded and a transient time is considered before starting averages for two-phase flows. The particulate flow is considered to be fully resolved when the particle radius contains at least 6 grid points corresponding to $R = 0.59\lambda = 10\eta$. The particle volume fraction is 3%. To obtain converged particle statistics, simulations are carried out over 12 large eddy turn-over times. In the present paper three different simulations are presented for solid to fluid density ratio ρ equal to 1, 2 and 4. No gravity effect is considered.

A study of the spatial spectrum has been carried out to verify that the presence of particles has only a minor influence on the turbulence statistics. In figure 2, the single phase flow spectrum of energy is compared to two-phase flow simulations for the three density ratios. Only slight modifications are observed at wavenumbers higher than the inverse of the particle radius. The energy spectrum is formed over the entire domain (accounting for the solid body motion of the particles).

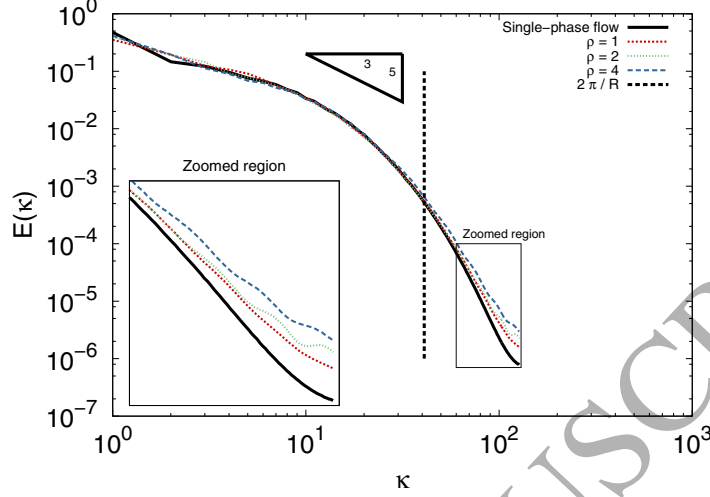


FIGURE 2. Energy spectra with and without particles. Solid line for single phase flow DNS. Dotted, dash-dotted and light dashed lines stand for density ratio equal to 1, 2 and 4 respectively. The vertical dash line represents the wavenumber corresponding to the particle diameter. Inset is a close-up for high wavenumbers content of spectra.

As shown by [26], the inclusion of the solid domain creates some oscillations on the wavenumbers larger than the inverse of the particle radius. As shown in figure 2, our simulations stand in a very dilute regime yielding these oscillations to be negligible. Linear forcing is made without taking into account the density ratio of the particles, equation 9. For this reason the energy on the entire domain increases when ρ increases. Because the case considered is very dilute only a weak increase of energy at high wavenumbers is observed.

In order to confirm the weak effect of the particles on the carrying fluid turbulence (the local effect will be discussed later) and overtake the problem of the computation of the spatial spectrum including grid points inside the particles, the temporal Lagrangian spectrum has been computed.

This spectrum is computed from 200000 Lagrangian fluid elements (point particles following the flow) which are randomly seeded in the fluid domain. Their trajectories are integrated while the turbulent suspension is simulated. Then, the Lagrangian velocity auto-correlation function, $R_L^f = \frac{\langle \mathbf{V}_i(t_0) \cdot \mathbf{V}_i(t_0 - t) \rangle}{\langle \mathbf{V}_i(t)^2 \rangle}$, is computed from those trajectories

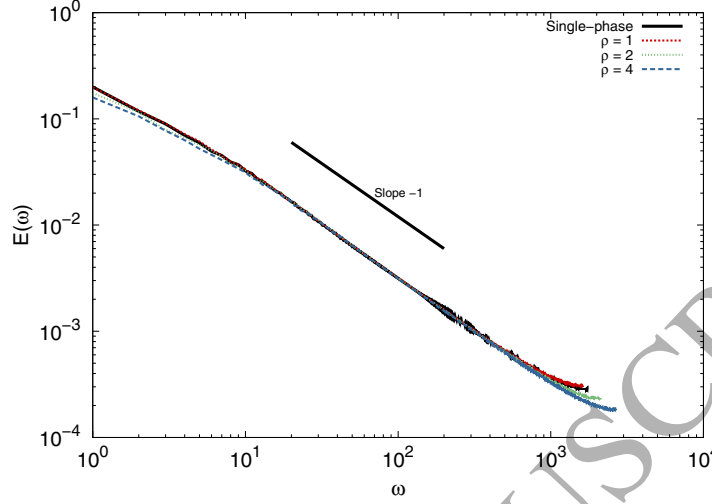


FIGURE 3. Temporal spectrum of the single phase simulation and three configurations of two-phase flows. These spectra were computed from tracer particle trajectories. Solid line for single phase flow DNS. Dotted, dash-dotted and light dashed lines stand for density ratio equal to 1, 2 and 4 respectively.

to evaluate the energy temporal spectrum $E(\omega) = \frac{1}{2} \mathfrak{F}(R_L^f) \mathfrak{F}^*(R_L^f)$. Where, \mathfrak{F} and \mathfrak{F}^* are the Fourier transform and its conjugate. The Lagrangian spectrum is given in figure 3. This statistical quantity is really a measure of the turbulence of the carrying flow and is not flawed by accounting simultaneously the fluid and solid in statistics. Based on figure 3, we can conclude that the carrying flow statistics remain constant for the three considered density ratios.

To characterize the particle response to fluid flow fluctuations, two different Stokes numbers are determined, based on the Kolmogorov time scale and the large eddy turnover time. The Stokes number based on the Kolmogorov time scale is relatively large $St_k = \{26, 52, 104\}$, as a consequence, the particles are inertial relative to the Kolmogorov scales. The preferential concentration of inertial particles in low vorticity regions has been commonly observed and quantified for small particles (pointwise or particles smaller than the Kolmogorov length scale). Particles whose Stokes number based on the Kolmogorov time scale are near unity are experiencing strong preferential concentration. Indeed to our knowledge, nothing on preferential concentration has been published with particle resolved simulations. For our simulations,

the Stokes number based on the large eddy turnover time is less than 10 ($St_E = \{1.5, 3.0, 6.0\}$) meaning that the time associated to the particles is equivalent to this flow time scale. Even for this intermediate scale no clusters formation was observed. Statistics on the radial pair distribution function did not show evidences of preferential concentration. Different explanations can be proposed. The first one is that the simulation time (12 eddy turn-over times) is not long enough for the particles to migrate in accumulation zones. The second explanation is that the physical life-time of the low vorticity regions at large scales is too short to give enough time for the particles to cluster. The segregation and clustering of finite size particles is still an open subject to study.

3.2. Particle statistics. The dynamics of particles smaller than the Kolmogorov scale has been studied extensively. Characterizing the relation between the particle statistics (kinetic energy and the velocity autocorrelation time) and the turbulence properties has been established in [41, 19, 12, 24, 15]. In table 1 statistics are reported for finite-size particles and scaled by the fluid tracer statistics. As expected the particle kinetic energy, averaged over the N_p particles during N_t time steps $q_p^2 = \frac{1}{2} \frac{\sum_j \sum_i \mathbf{V}_i^2(t_j)}{N_t N_p}$, is reduced when the density ratio increases while the velocity autocorrelation time increases. This reduction is predicted by Tchen-Hinze theory [41, 19]:

$$(10) \quad \left(\frac{q_p^2}{q_f^2} \right)_{T.-H.} = \frac{\frac{T_L^f}{\tau_p} + b^2}{\frac{T_L^f}{\tau_p} + 1}$$

where, $b = \frac{3\rho_f}{2\rho_p + \rho_f} = \frac{3}{2\rho + 1}$.

However, the particle kinetic energy is less important than the prediction of the Tchen-Hinze theory, $\left(\frac{q_p^2}{q_f^2} \right)_{T.-H.}$. Indeed, Tchen-Hinze theory is based on an estimate of the fluid kinetic energy at the position of particles assuming that their size is much smaller than the Kolmogorov length scale. In our case, the particles are significantly larger than the Kolmogorov length scale therefore they are not experiencing the full fluid fluctuations (large particles behave like a spatial low pass filter of the flow kinetic energy).

The Lagrangian velocity autocorrelation time $T_L = \int_0^\infty R_L(t) dt = \int_0^\infty \frac{\langle \mathbf{V}_i(t_0) \cdot \mathbf{V}_i(t_0 - t) \rangle}{\langle \mathbf{V}_i(t)^2 \rangle} dt$ is presented in table 1. This autocorrelation time T_L is normalized by the autocorrelation time of the fluid particles T_L^f obtained thanks to the autocorrelation function R_L^f (see section 3.1).

| ρ | $\frac{q_p^2}{q_f^2}$ | $\left(\frac{q_p^2}{q_f^2}\right)_{T.-H.}$ | $\frac{T_L}{T_L^f}$ |
|--------|-----------------------|--|---------------------|
| 1 | 0.85 | 1 | 1.31 |
| 2 | 0.79 | 0.5 | 1.45 |
| 4 | 0.74 | 0.2 | 1.65 |

TABLE 1. Particle statistics.

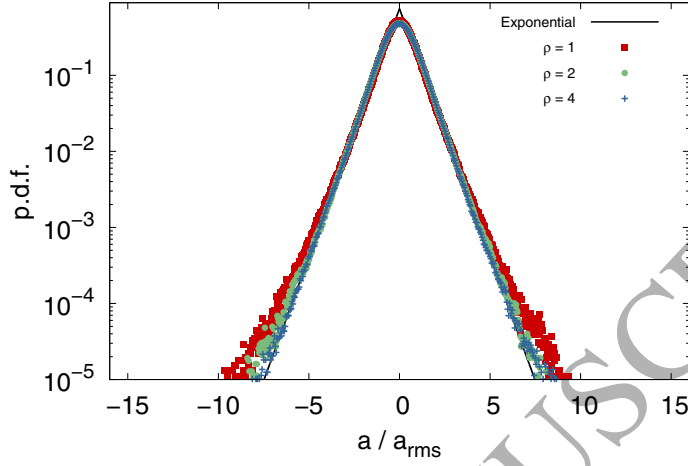
It characterizes the typical time a particle takes to change its velocity direction. The present simulations show that T_L increases as density ratio rises. Similar trend is observed for inertial point-particles simulations. As can be seen in table 1, whatever the density ratio is, even for neutrally buoyant particles, the normalized autocorrelation time is greater than 1, clearly showing finite size effect.

Analysing the acceleration statistics provides insights on the dynamic response of particles to the turbulence forcing. It has been shown in literature [46, 31, 8] that the probability density function of finite size solid particles acceleration $P(a)$ can be approximated by an exponential law $\exp^{-|a|^\beta}$ where $\beta \leq 1$. As showed by [3] the constant β approaches unity for inertial particles (here for high density ratio ρ). In figure 4 a) and b) two p.d.f. of particle accelerations normalized by their r.m.s. values have been reported for the different simulations. In figure 4 a) the p.d.f. has been obtained without considering the acceleration occurring during collisions. For this case, the p.d.f. closely follows an exponential law with $\beta = 1$ whatever the density ratio. Therefore, this is a measure of acceleration statistics strictly related to the interaction with turbulence in the very dilute regime (no collision).

Concerning, the case where acceleration during collision is taken into account for the p.d.f. acceleration (figure 4 b), the same exponential behaviour is observed for low acceleration values. This is no longer the case for larger values. Indeed the tails of the p.d.f. in figure 4 b) are shifted towards higher values. This is related to rare but strong collision events on the acceleration.

In [31] an experimental study has been conducted on the interaction between finite size soap bubbles and turbulent air channel flow. It was shown that the r.m.s. acceleration scaled by the fluid dissipation rate ($A_0 = a_{r.m.s.}^2 / \varepsilon_t^{-3/2} \nu^{1/2}$) decreases as ρ increases. In order to compare to this result the dissipation of the turbulent flow ε_f is estimated in the present simulations from the spectrum: $2\nu \int_0^\infty \kappa^2 E(\kappa) d\kappa$. In [31] an exponential decrease has been observed from $\rho = 1$ to $\rho = 10$ as $A_0 = 2.8\rho^{-0.6}$. From our simulations the same trend can be observed as $15\rho^{-0.94}$ (figure 5).

a)



b)

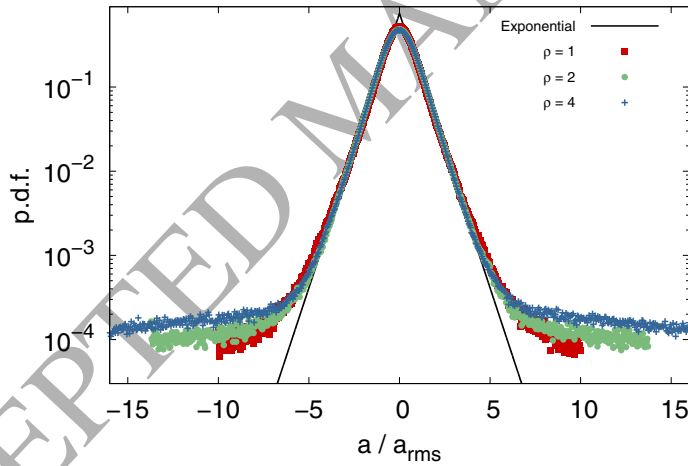


FIGURE 4. Probability density function of particle acceleration. Exponential p.d.f. is given as a reference, $\exp^{-|a|^\beta}$, $\beta = 1$. a) without collision events. b) with collision events.

4. DISSIPATION DISTRIBUTION AROUND PARTICLES

4.1. Moving frame around particles. To evaluate the average flow around moving particles a specific post-processing has been applied to instantaneous DNS flow fields. A local framework is attached to each

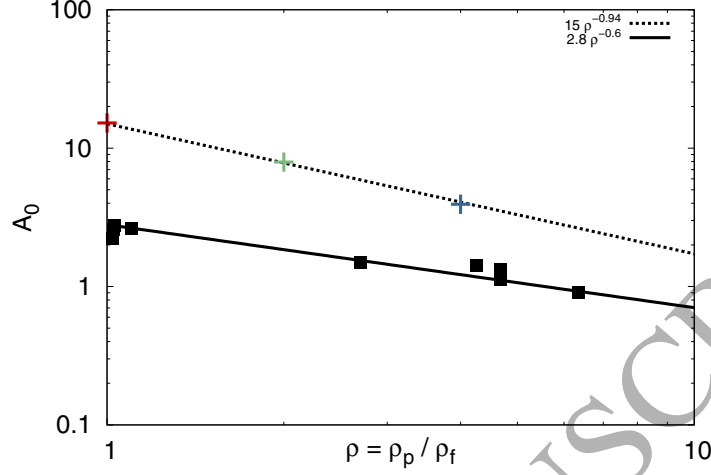


FIGURE 5. Dimensionless acceleration r.m.s. compared to density ratio. Present simulations (cross) and experiments of Qureshi [31] (squares) and their respective exponential law.

particle center and it is translated with the particle velocity. A unit vector is aligned with the instantaneous particle velocity $\mathbf{e}_{\mathbf{v}_p} = \frac{\mathbf{v}_p}{\|\mathbf{v}_p\|}$. As the average flow is axis-symmetric, this flow field is described in the moving particle framework in a $\{r, \theta\}$ plane, with r the distance to the particle center and θ the angle with the unit vector. A staggered polar grid is attach to the particle framework. The radial distribution $\{r_i\}$ is refined near the particle surface to provide a better description of boundary layers. The angle increment is also not uniform to keep rather constant the volume of each cell for a given radii r_i . This choice is made in order to converge smoothly the statistics for each cell. The surface of the cell between θ_j and θ_{j+1} is approximated by $2\pi r_i \sin\left(\frac{\theta_j + \theta_{j+1}}{2}\right) d\theta_j$. In our case 180 angles are used in the $[0..180]$ interval.

The different steps of the post-processing are the following:

- (1) The DNS flow field is known on the staggered fixed Cartesian grid.
- (2) For each radius r_i a spherical shell around the particle is defined. The values of the physical quantities (velocity, dissipation...) are linearly interpolated at the intersection between the spherical shell and the Cartesian grid using the surrounding Cartesian grid values.

- (3) For each interpolation location, the angle between $\mathbf{e}\mathbf{v}_p$ and the radius connecting this location with the particle center is computed. Then, the value is added to the average of the cell which node is referenced by $\theta \in [\theta_j, \theta_{j+1}]$.

This algorithm is applied for each particle and for many time steps chosen arbitrarily to obtain converged statistics.

In figure 6 the streamlines resulting from the average velocity flow around particles are presented for different density ratios $\rho = 1, 2$ and 4.

As shown by [9] the absence of fore-and-aft symmetry is related to the conditional averaging of the flow in a framework moving with the particle. This has been observed also for flow around a tracer particle in [9].

4.2. Dissipation rate in a moving frame around particles. An important feature of two-phase turbulence is that the presence of particles generates modulation of turbulence. Depending on the particle properties and the flow configuration, particles can enhance or damp fluid flow turbulence (this fundamental question is still open). Fully resolved simulations of finite size particles provide information which cannot be obtained with point-wise two-way coupling simulations. The dissipation of energy is a local effect occurring near the particle surface and in its wake.

The dissipation $\varepsilon = 2\nu \left(\frac{\partial u_i}{\partial x_j} + \frac{\partial u_j}{\partial x_i} \right)^2$ is computed on the Cartesian grid and averaged as presented in the previous paragraph. Figure 7 shows the spatial distribution of dissipation scaled by ε_∞ which is the overall turbulent dissipation of the flow. A peak of dissipation is located in the front of the particle. In the present simulations this peak reach 2.5 the average fluid dissipation. The magnitude of this dissipation increases with density ratio. This is the result of the progressive decorrelation of the particle velocity and the local flow which increases for large particle density. The dissipation increases around particles over a distance smaller than one radius in agreement with different authors.

In the experiments of [40] the dissipation around a sedimenting particle in a turbulent flow is given. The particles fall in a turbulence chamber. The particles are much heavier than the surrounding gas and their radii are similar to the Kolmogorov length scale. The turbulence around the particles are measured by a PIV system. In this experiment the dissipation observed around the particles has increased to 3.5 times the turbulence dissipation.

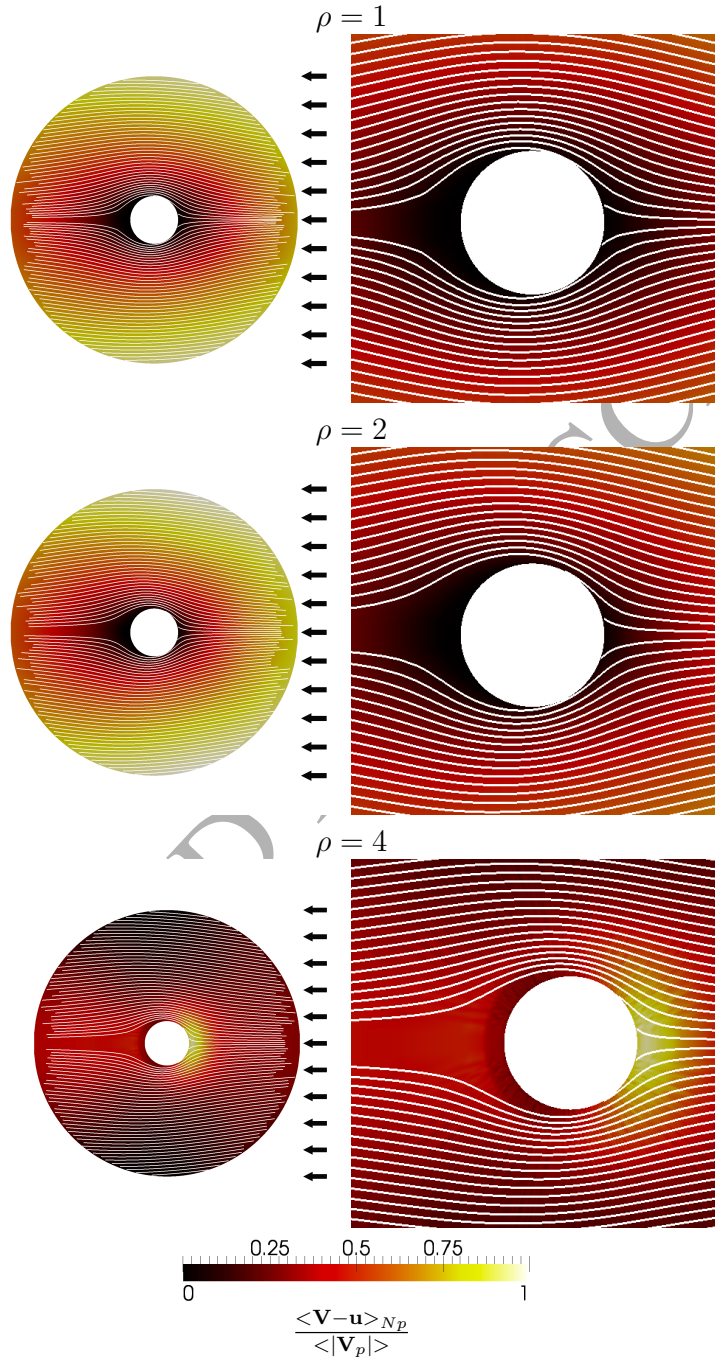


FIGURE 6. Intensity of the average relative velocity and streamlines around a reference particle for each two-phase flow configuration.

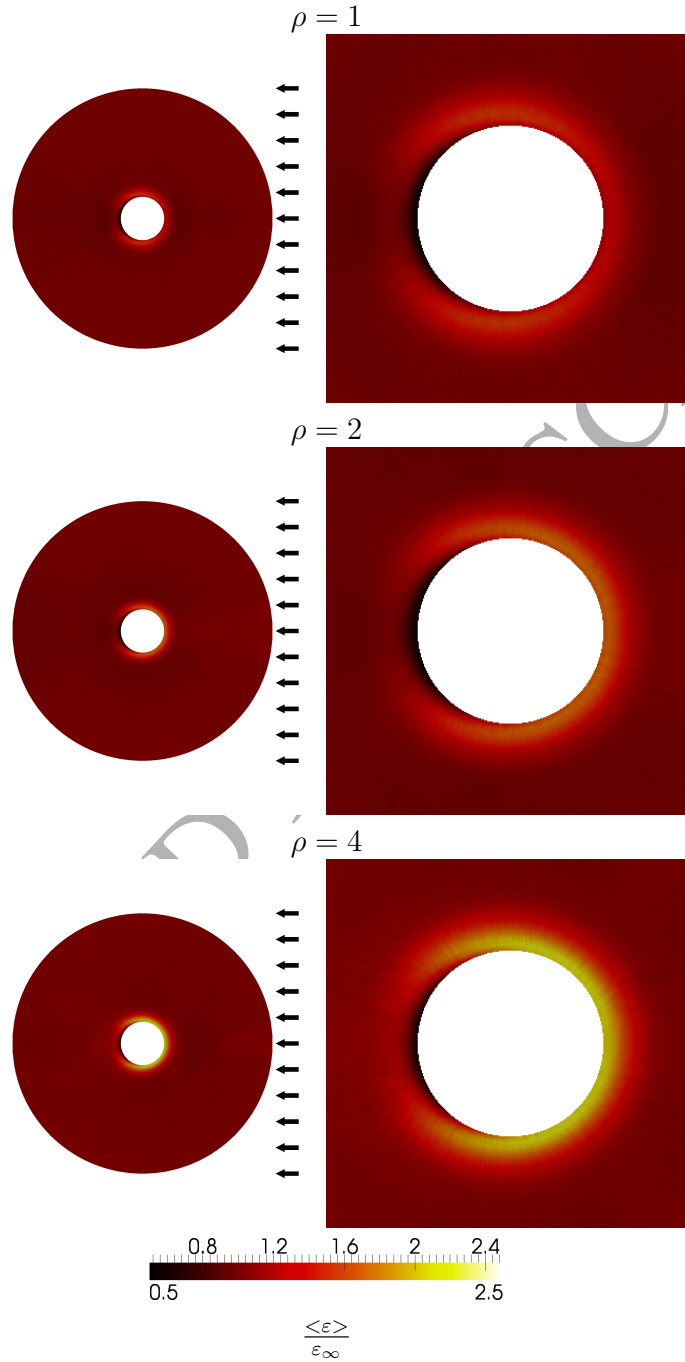


FIGURE 7. Spatial distribution of average dissipation for each two-phase flow configuration (left column). Close-up around the particle surface (right column). Left: complete average domain. Right: detail around the particles.

Numerically, several studies have been conducted. In the simulations of a turbulent particle laden flow presented by [42] instantaneous dissipation fields are presented. It could be seen that the local dissipation increases around the particles. In this paper, no average dissipation is provided. In [29] a fixed particle with radius 4 times the Kolmogorov scale is simulated in a fully turbulent flow. The averaged dissipation for a given distance is computed showing an increase of the dissipation around 4 times the averaged dissipation at a distance of one radius. The averaged dissipation for a given distance is also provided by [47] for simulations with free particles in a turbulent flow for the same particle size ($R = 4\eta$) and for a density ratio $\rho = 4$. The method used is based on the Lattice-Boltzmann method. In this case the dissipation is 6 times larger around the particles than the averaged dissipation in the fluid.

In [26] simulations of finite size particles are carried out with the IBM method for different radii $R \in [8.2..17.7]$ and density ratios $\rho \in [2.53..10]$. They computed the averaged dissipation for a given distance for two regions of the flow: the front of the particles (equivalent to $\theta \in [0..90]$ in the present notation) and the back of the particle ($\theta \in [90..180]$). As in the present paper, the dissipation in the front of the particle is larger and the influence is observed over one radius distance.

Finally, [9] provides a detailed study of slipping velocity and local dissipation around buoyant particles in a turbulent flow. This numerical study is based on a pseudo-spectral Navier-Stokes solution and an IBM method to account for fully-resolved particles. Different radii are considered ($R \in [8.5..33.5]\eta$) that permit to study the influence of the particles size. In this case the average of the dissipation is split in three regions: upstream ($\theta \in [0..45]$), transverse ($\theta \in [45..135]$) and downstream ($\theta \in [135..180]$). Again, the dissipation in the front of the particles is larger than at the rear. On the three regions the increase of dissipation is limited to one radius.

The magnitude of dissipation (front and rear of particles) has been compared in figure 8 with the results of [26] and [9]. The profiles of dissipation at the front and at the rear of the particles are reported.

The orders of magnitude of dissipation found in the literature from the surface of the particle to 3 times the particles radius are similar to our computations. In addition, for all the cases we observe that the dissipation increase is less important at the particle rear. As in [26] the dissipation peak increases with the density ratio.

Even if there are major differences between the way the computations are carried out, the numerical approach and the simulation parameters,

the magnitude of the dissipation increase agrees. Nevertheless, dissipation seems to be greater for the buoyant case of [9] than for our simulations. We explain this difference because the particles are larger than in our simulations, $R = 17\eta$ instead of $R = 10\eta$, and thus, they are more inertial. Another explanation could be that the turbulence is stronger than in the present simulations, $Re_\lambda = 160$.

As a conclusion, the present simulations confirm the results obtained by several authors [27, 9, 29, 40]: the particles modify locally the turbulence. This modification is always an increase of the local dissipation of the turbulence. This dissipation is larger in the front of the particles and its spatial extension is less than one radius. The magnitude of this dissipation increases with particle inertia.

5. COLLISION STATISTICS

5.1. Collisions with solid contact only. Understanding the collision dynamics is a key point for modelling suspension flows and predicting coalescence events for drops. In this section, only the solid-solid model has been activated without lubrication (eq. (6)).

We have followed the present procedure to form statistics. If we call Δt_{coll} the time between two collisions for a given particle, and $\Delta t_{coll,i}$ the averaged of all the Δt_{coll} concerning the i^{th} particle, the inter-collision time τ_c for N_p particles is defined as $\tau_c = \langle \Delta t_{coll,i} \rangle_{N_p} = \frac{1}{N_p} \sum_{i=1}^{N_p} \Delta t_{coll,i}$. Another way to compute τ_c is to count the number of collision N_{coll} during the total time of analysis ΔT , and for the N_p particles to obtain $\tau_c = \frac{N_p}{2N_{coll}} \Delta T$.

This characteristic time can be estimated theoretically (eq. 11) from the average relative velocity of particles $\langle |w_r| \rangle$ as proposed in [36].

$$(11) \quad \frac{1}{\tau_c} = \frac{1}{2} g_0 n_p^2 \pi (2R)^2 \langle |w_r| \rangle$$

When the motion of particles is fully uncorrelated, the relative velocity of particles $\langle |w_r| \rangle$ can be evaluated from the particle kinetic energy q_p^2 , [1] :

$$(12) \quad \frac{1}{\tau_c^{th}} = \frac{1}{2} g_0 n_p^2 \pi (2R)^2 \sqrt{\frac{16}{\pi} \frac{2}{3} q_p^2}$$

In table 2 the inter collision time is reported for different density ratios. Two different inter collision times have been considered. The first one τ_c^{th} is obtained thanks to equation 12, by extracting the particle kinetic energy q_p^2 from simulations with the assumption that g_0 is

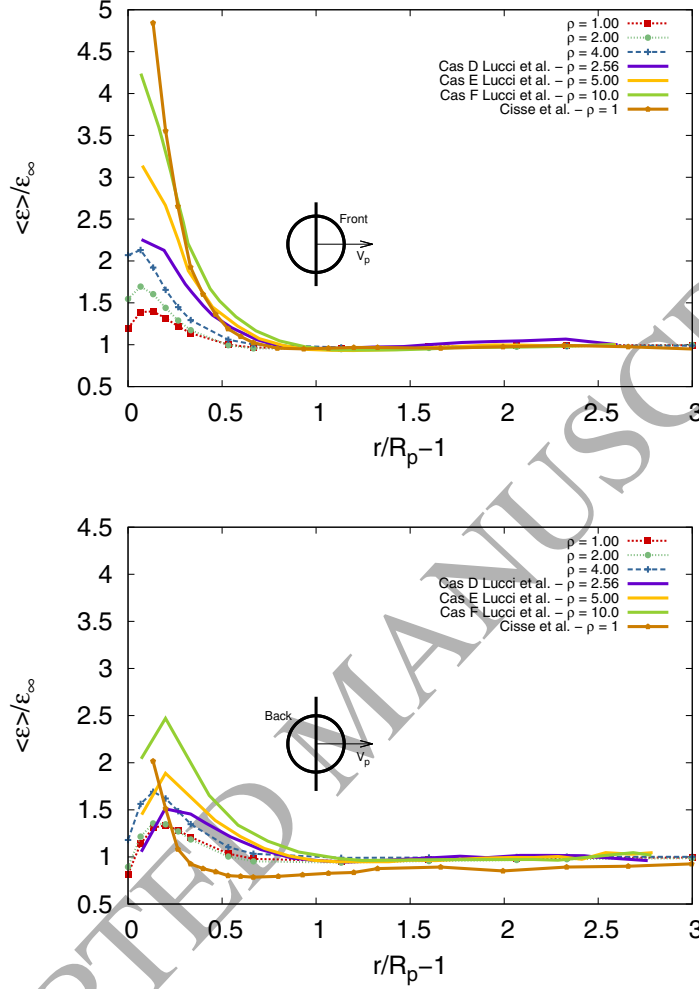


FIGURE 8. Dissipation in the front and at the rear of the particle. Present simulations compared to [26] and [9].

equal to 1 (particle dilute flow) and using the effective collision radius ($1.1R$ because the collision is activated for $\epsilon = 0.1$) and $n_p = \frac{512}{(2\pi)^3}$ the particles number density. The second inter collision time τ_c^n is directly obtained by estimating the time between two collisions in simulations. This estimate has been achieved with two methods:

$\tau_c^{n,1}$ We average all the times between the end of a collision and the beginning of the next collision for all the particles. In this

| ρ | $\left[\frac{\tau_c^{n,1}}{\tau_k} \dots \frac{\tau_c^{n,2}}{\tau_k} \right]$ based on computations | $\frac{\tau_c^{th}}{\tau_k}$ theory eq. (12) |
|--------|---|---|
| 1 | [22.6 .. 24.5] | 21.5 |
| 2 | [19.3 .. 20.8] | 22.4 |
| 4 | [16.2 .. 17.1] | 23.1 |

TABLE 2. Comparison of inter collision times for various density ratios. The reference Kolmogorov time is $\tau_k = 0.0635 s$

estimate the solid contact, which is not instantaneous with our soft sphere model, is not taken into account.

$\tau_c^{n,2}$ Is the ratio between the total number of collisions occurring during the simulation and the simulation time.

The first method gives a lower bound of τ_c while the second one provides an upper bound.

The orders of magnitude of inter collision times are comparable whatever method used. The gap between τ_c^{th} , $\tau_c^{n,1}$, $\tau_c^{n,2}$ is always less than 15%. As expected from equation (12), τ_c^{th} is increasing with the density ratio as q_p is decreasing. In contrast, the collision time measured is decreasing with increasing density ratio. One can explain this behaviour by considering that the evaluation of τ_c^{th} is done under the assumption of $g_0 = 1$.

In order to understand those discrepancies the probability density function of inter-collision times is now considered. In simulations, the p.d.f. is obtained by counting the number of occurrences of each inter collision time Δt_{coll} for all the particles. The p.d.f. is divided by the total number of occurrences. From the kinetic theory of granular flows (uncorrelated motion of particles) the p.d.f. follows

$$(13) \quad P(\Delta t_{coll}) = \frac{1}{\tau_c^{th}} \exp\left(-\frac{\Delta t_{coll}}{\tau_c^{th}}\right)$$

In figure 9, the probability density function is reported for three density ratios. A comparison is provided between simulations and kinetic theory.

The p.d.f. obtained with simulations follows the kinetic theory for $\Delta t_{coll} < 4\tau_c$. For larger values of Δt_{coll} , the measured p.d.f. has a large dispersion due to the small number of occurrences that are counted. For this reason, the comparison to the kinetic theory is not representative for $\Delta t_{coll} > 4\tau_c$.

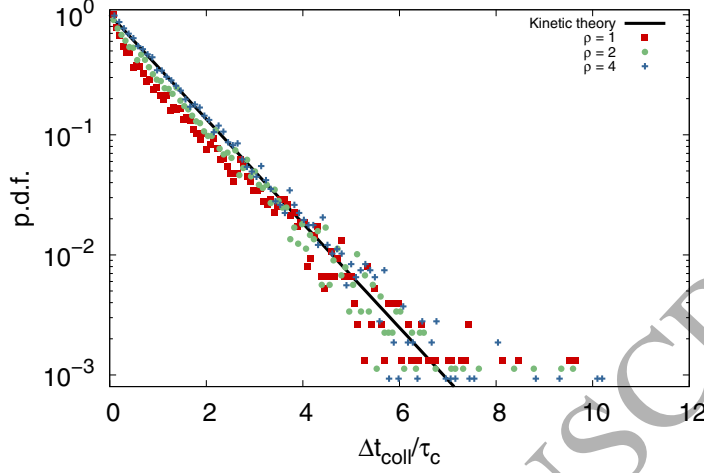


FIGURE 9. Inter-collision time probability density function. Solid line corresponds to equation (13), ($\tau_c = \tau_c^{th}$ for kinetic theory and $\tau_c = \tau_c^{n,1}$ for the measured p.d.f.).

If we focus on the small inter collision times, the comparison between kinetic theory and measured p.d.f. shows a larger difference for $\rho = 1$ than for $\rho = 4$. This is the consequence of the particle motion that follows more easily the flow and comes into contact with slightly more correlated trajectories when $\rho = 1$. This discrepancies for $\rho = 1$ could be inferred to the effect of secondary collisions that will be affected by the lubrication model. A discussion on the secondary collisions is given in section 5.2.

In order to describe more precisely the collision regime, statistics of the velocity orientations when collision occurs are analysed. For uncorrelated motion of particles, the p.d.f. of the angle between two particle velocities at contact is predicted by [24]:

$$(14) \quad f(\theta_{coll}) = \frac{\int_0^\infty \int_0^\infty 8\pi \sin(\theta_{coll}) V_a^2 V_b^2 \sqrt{V_a^2 + V_b^2 - 2V_a V_b \cos(\theta_{coll})} f_v(V_a) f_v(V_b) dV_a dV_b}{\int_0^\pi \int_0^\infty \int_0^\infty 8\pi \sin(\theta) V_a^2 V_b^2 \sqrt{V_a^2 + V_b^2 - 2V_a V_b \cos(\theta)} f_v(V_a) f_v(V_b) dV_a dV_b d\theta}$$

where f_v is the velocity p.d.f..

In figure 10 the kinetic theory corresponding to equation 14 for the collision angle p.d.f. is compared to simulation results. A Gaussian profile has been used for f_v corresponding to the behaviour measured in our simulations.

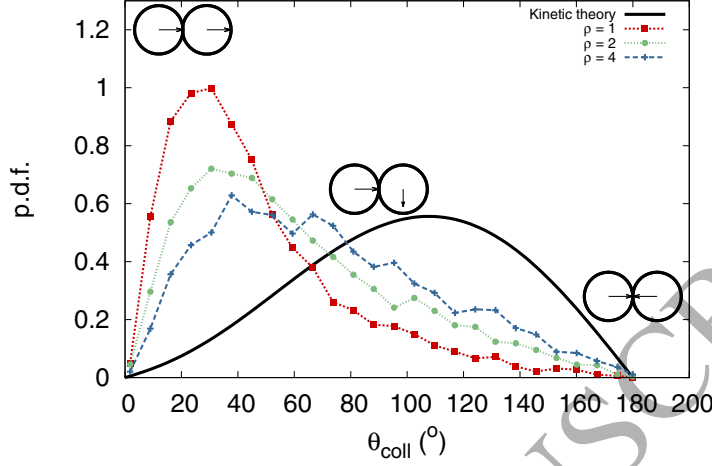


FIGURE 10. Probability density function of the angle between particle velocity at contact. Theory for uncorrelated motion is given by equation (14) (solid line). A sketch of particle velocity at contact is provided for $\theta_{coll} = \{0, 90, 180\}$ degrees.

Whatever the density ratio is, the maximum of the measured p.d.f. is obtained for $20^\circ < \theta_{coll} < 40^\circ$, whereas the kinetic theory provides a peak at 108° . This is characterized by a shift of the p.d.f. from large to low angles indicating that particles come into contact with nearly parallel velocities, evidencing a particle to particle trajectory correlation. This shift decreases for higher density ratio showing that particle inertia yields larger decorrelation between the particles and the carrying fluid flow. From this result, it is obvious that the relative velocity at contact should be lower than the one obtained with the kinetic theory discussed below.

We now compute the relative velocity at contact $w_r = 2u_{n,coll}$, where $u_{n,coll}$ is the relative velocity given by equation (5) at the beginning of contact. For uncorrelated velocity particles with a Gaussian velocity distribution, the p.d.f. of w_r is given by

$$(15) \quad f_{coll}(|w_r|) = \frac{2}{(8/3q_p^2)^2} |w_r| \exp\left(-\frac{|w_r|}{8/3q_p^2}\right)$$

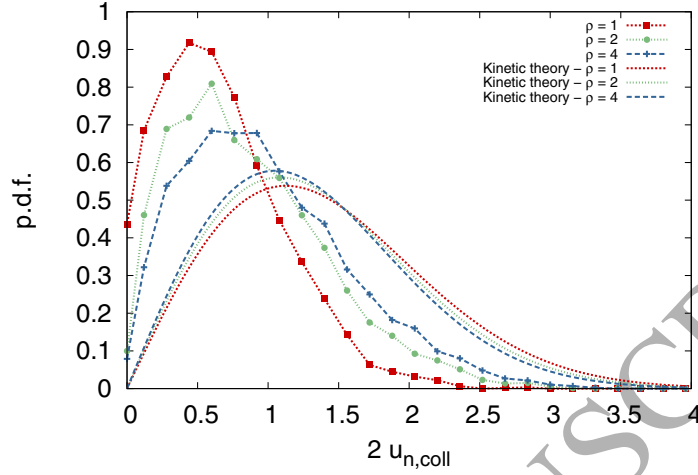


FIGURE 11. Probability density function of the relative velocity at contact (theory and simulations).

In figure 11, we compare the p.d.f. of the relative velocity at contact obtained with the kinetic theory and simulation results. In equation (15), the kinetic energy q_p^2 is obtained from the simulations.

As already observed for p.d.f. of the angle, a clear shift of the p.d.f. of velocity is also reported in simulations compared to the kinetic theory. As expected, the relative velocity at contact is lower in the simulations than in an uncorrelated motion. Particle inertia increases decorrelation of particle motion and fluid flow yielding a better agreement with kinetic theory for the largest density ratio.

The relative velocity at contact characterizes the energy involved in collisions. When collisions occur in a viscous fluid, part of this energy is dissipated by viscous effect during the fluid drainage. As a result, the velocity after the collision is reduced. It has been shown that the impact Stokes number defined as $St_{coll} = \frac{2 R u_{n,coll} \rho_p}{9 \mu}$ is a dimensionless parameter which can determine the collision regime (from dry contact to viscous rebound). In order to estimate the energy dissipated during the collision the restitution coefficient e is defined as the ratio between the velocity after the collision and before the collision. Based on experiments, the correlation proposed by [25], $\frac{e}{e_d} = \exp\left(-\frac{35}{St_{coll}}\right)$, gives the relation between the restitution coefficient and the Stokes number (the restitution coefficient is scaled by its value for a dry contact e_d). In figure 12 the p.d.f. of impact Stokes numbers is presented as well

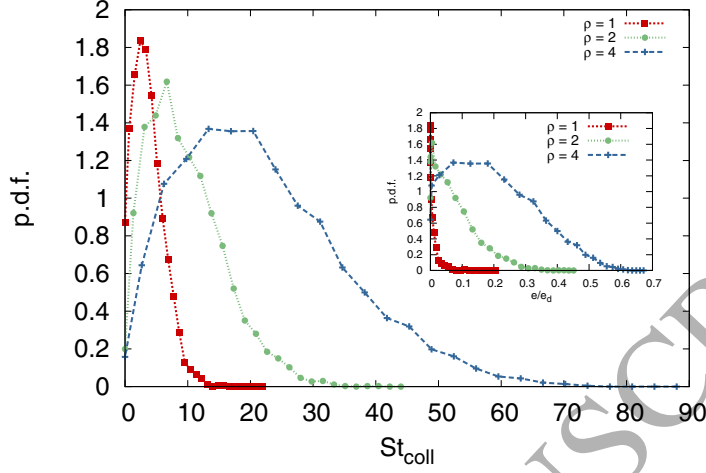


FIGURE 12. Probability density function of the impact Stokes number obtained from the relative velocity. Inset plot represents the p.d.f. of the restitution coefficient obtained with the correlation given by [25].

as the distribution of the effective restitution coefficients based on the p.d.f. of the relative velocity, figure 11.

It can be seen that for the case $\rho = 1$ most of collisions are in the Stokes range corresponding to no rebound ($e \simeq 0$). Rebound will not occur and particles will stay stuck together. For the case $\rho = 4$ the values of the Stokes numbers cover a wide range corresponding to restitution coefficients lower than 0.5. This means that for the range of physical parameters we simulated, lubrication effects during particle encounters are important and must be accounted for.

5.2. The effect of lubrication on collision statistics. The effect of lubrication on collisions will be studied for cases $\rho = 1$ and $\rho = 4$. The lubrication model corresponding to equation (8) is now activated at distance $1.1 R$ similarly to the solid-solid model in the previous section. The solid-solid collision model is not modified and is activated only for the particles that overlap.

Several physical quantities and statistics will be compared in order to highlight the effect of film drainage on collisions. The kinetic energy of particle agitation, the autocorrelation time, the velocity and acceleration distributions are not drastically modified by including the effect of lubrication. A first difference between simulations with and without lubrication model appears on the averaged distance between particles.

For example, the mean distance to the nearest neighbour is decreased by about 5%, [21]. The same result can be observed in the radial distribution function: for small distances the probability to observe a particle increases, meaning that particles tends to stay closer to each other. The activation of lubrication between two particles decreases the relative velocity between them during the encounter yielding a longer time of nearby interaction.

Here we focus on the modification of the collisional regime. In order to analyse this collisional regime it is necessary to make the difference between two different interactions: the encounter, defined as the activation of lubrication model, and the solid-solid collision, defined as the activation of solid-solid model.

The inter-encounter time obtained as the average time between two activations of the lubrication model is $\{21.6, 16.1\} \tau_k$ for $\rho = \{1, 4\}$ respectively. The elapsed time between two successive interactions is close to the results obtained for the simulations without lubrication model: $\tau_c^{n,1} = \{22.6, 16.2\} \tau_k$. It shows that the encounters between particles do not depend on the lubrication model but only on the flow dynamics which carries the particles towards contact. In figure 13 the p.d.f. of the inter-encounter and inter-collision times are presented for the simulations with and without lubrication model.

In all cases an exponential decay is observed for large inter collision or inter encounter times. This is resulting from the uncorrelated motion in agreement with the kinetic theory.

When the lubrication is considered, the ratio of collisions occurring at small times increases. As a consequence, the level of the exponential law decreases. For the small inter collision times the exponential law is no more valid. This effect is enhanced for $\rho = 1$, but also present for $\rho = 4$. Because of the increase of small Δt_{coll} occurrences, the inter collision time $\tau_c^{n,1}$ is reduced from $22.6 \tau_k$ to $2.5 \tau_k$ for neutrally buoyant particles. This is explained by the occurrence of many body solid-solid collisions during the activation of the lubrication model. The lubrication slows down the particles during separation after a collision, increasing solid-solid collision events. These phenomena have been also reported in [42], so-called secondary collisions.

As proposed by [42] the p.d.f. can be split into two contributions. The first one, relative to primary collisions has an exponential tail corresponding to long time collisions: $P(\Delta t) = \frac{\alpha}{\tau_c} \exp\left(-\frac{\Delta t_{coll}}{\tau_c}\right)$. The second one, relative to secondary collisions is obtained as the difference between the overall p.d.f. and the first contribution. α is a parameter representing the gap between the real p.d.f. and the kinetic theory.

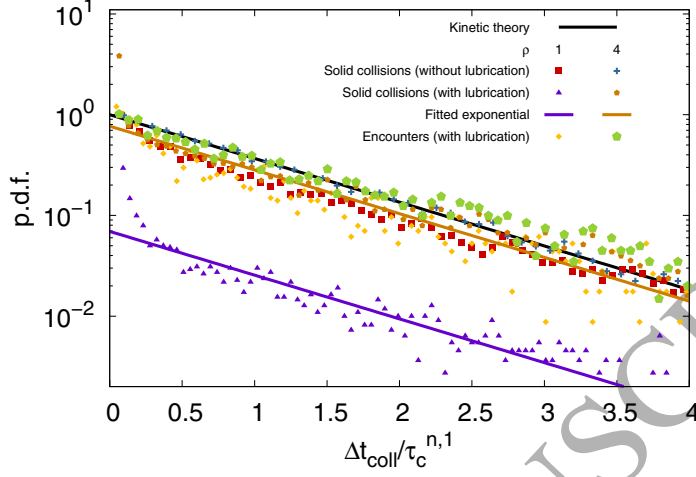


FIGURE 13. Inter-collision time probability density function for simulations with and without lubrication model. Fitted exponential law is given for solid-solid collisions for simulations with lubrication model. For comparison purpose the Δt_{coll} time is scaled by the inter collision time obtained without lubrication model (see table 2). The kinetic theory (equation (13)) corresponds to solid line.

It is obtained by fitting the p.d.f. for long inter-collision times. The exponential law of the kinetic theory is recovered when $\alpha = 1$.

From our simulations we obtain α for the solid-solid collisions with the lubrication model:

- For $\rho = 1$, $\alpha = 7\%$: only 7 paths over 100 are reproduced by the kinetic theory, the other 93 are free paths between secondary collision. In the simulations of [42], α was ranging between 8% and 11% which agrees with our results.
- For $\rho = 4$: the occurrence of consecutive collisions is less pronounced. The inter-collision time is reduced only from $16.2 \tau_k$ to $14.6 \tau_k$. The parameter α is equal to 77%. Here, particle inertia drives the particles towards more energetic collisions and rebounds. The effect of lubrication is weaker and cannot keep the particles together after collision.

6. CONCLUSION

The present paper provides an analysis of a sustained turbulent flow seeded with finite-size particles based on fully resolved simulations. Based on a numerical method previously developed for this kind of simulation [44, 6], specific characteristics of the particle flow have been investigated such as the local dissipation around particles and the collision dynamics. These phenomena were under interest as only few works were devoted to them in the literature. Three configurations were simulated with different density ratios.

From a macroscopic point of view simulations have provided the following results: First of all, Eulerian as well as Lagrangian turbulent energy spectra are reported. It has to be noticed that the later has never been achieved with resolved scale simulations. The conclusion is that whatever the density ratio the energy spectra are almost the same, with only small differences at the largest and smallest scales. Otherwise, the acceleration of the particles is modified by the inertia and the collisions. This second effect is observed on the acceleration p.d.f. and was not reported in previous works.

A specific point of interest in the present work was the averaged dissipation around particles. Simulations confirm that dissipation increases near the particle. On one hand, dissipation is concentrated in the front of the particle and is extended over one radius. On the other hand, dissipation increases with the particles inertia, almost 2 times the fluid turbulent dissipation.

The collision regime was also analysed in this paper. First of all, it is shown that when particle inertia increases the collisions can be described by kinetic theory. This is verified for the p.d.f. of the inter collision time, the angle of the collision and the relative velocity at contact. These two last statistics were not often studied and provide interesting physical information. The divergence between measured p.d.f. and the kinetic theoretical p.d.f. for the less inertial particles are here explained: the particle pair velocities are correlated when they are near each other. This is an effect of their correlation with the surrounding fluid velocity. The particle to particle correlations have a strong influence on the energy of the collisions which decreases, specially for neutrally buoyant particles. For this last configuration, the measured impact Stokes number is near the sticking particle configuration. The sticking effect can be interpreted as a lack of rebound that is produced by energy dissipation due to lubrication. This is confirmed by a comparison of the simulation with and without lubrication model. This study shows that for neutrally buoyant particles the lubrication

force prevents particles to separate after the solid collision. Thus, several solid collision appears after the final separation. That could have many effects on physical applications, for example on the creation of aggregates.

Acknowledgement - We are grateful for access to computational facilities of CINES and CCRT under project number x20162b6115. This work was also granted for HPC resources at CalMip under the project 2013-P0633. The authors thank P. Fede for fruitful discussions about collisional regimes.

REFERENCES

- [1] J. Abrahamson. Collision rates of small particles in a vigorously turbulent fluid. *Chemical Engineering Science*, 30(11):1371–1379, November 1975.
- [2] A. M. Ahmed and S. Elghobashi. On the mechanisms of modifying the structure of turbulent homogeneous shear flows by dispersed particles. *Physics of Fluids*, 12(11):2906, 2000.
- [3] J. Bec, L. Biferale, G. Boffetta, A. Celani, M. Cencini, A. Lanotte, S. Musacchio, and F. Toschi. Acceleration statistics of heavy particles in turbulence. *Journal of Fluid Mechanics*, 550:349, February 2006.
- [4] G. Bellani and E. A. Variano. Slip velocity of large neutrally buoyant particles in turbulent flows. *New Journal of Physics*, 14(12):125009, 2012.
- [5] M. Boivin, O. Simonin, and K.D. Squires. Direct numerical simulation of turbulence modulation by particles in isotropic turbulence. *Journal of Fluid Mechanics*, 375(1):235–263, 1998.
- [6] J. C. Brändle de Motta, W.-P. Breugem, B. Gazanion, J.-L. Estivalezes, S. Vincent, and E. Climent. Numerical modelling of finite-size particle collisions in a viscous fluid. *Physics of Fluids*, 25(8):083302, 2013.
- [7] H. Brenner. The slow motion of a sphere through a viscous fluid towards a plane surface. *Chemical Engineering Science*, 16(3-4):242–251, 1961.
- [8] E. Calzavarini, R. Volk, M. Bourgoïn, E. LéVêQue, J.-F. Pinton, and F. Toschi. Acceleration statistics of finite-sized particles in turbulent flow: the role of Faxén forces. *Journal of Fluid Mechanics*, 630:179, June 2009.
- [9] M. Cisse, H. Homann, and J. Bec. Slipping motion of large neutrally buoyant particles in turbulence. *Journal of Fluid Mechanics*, 735:null–null, 2013.
- [10] M. D. A. Cooley and M. E. O’Neil. On the slow motion generated in a viscous fluid by the approach of a sphere to a plane wall or stationary sphere. *Mathematika*, 16:37–49, 1969.
- [11] C. Corre, J. L. Estivalezes, S. Vincent, and O. Simonin. Direct numerical simulation of the motion of particles larger than the kolmogorov scale in a homogeneous isotropic turbulence. 2008.
- [12] E. Deutsch. *Dispersion de particules dans une turbulence homogène isotrope stationnaire calculée par simulation numérique directe des grandes échelles*. PhD thesis, Ecole Centrale de Lyon, 1992.
- [13] S. Elghobashi and GC Truesdell. On the two-way interaction between homogeneous turbulence and dispersed solid particles. i: Turbulence modification. *Physics of Fluids A: Fluid Dynamics*, 5:1790–1790, 1993.

- [14] M Elhimer, A Jean, O Praud, R Bazile, M Marchal, and G Couteau. Dynamics of finite size neutrally buoyant particles in isotropic turbulence. *Journal of Physics: Conference Series*, 318(5):052004, December 2011.
- [15] P. Fedé. *Modélisation et simulation de l'influence de la turbulence sur les collisions dans les écoulements mono- et bi-solides*. PhD thesis, Institut National Polytechnique de Toulouse, Toulouse, 2004.
- [16] A. Ferrante and S. Elghobashi. On the physical mechanisms of two-way coupling in particle-laden isotropic turbulence. *Physics of Fluids*, 15(2):315, 2003.
- [17] J.R. Fessler, J.D. Kulick, and J.K. Eaton. Preferential concentration of heavy particles in a turbulent channel flow. *Physics of Fluids*, 6:3742, 1994.
- [18] H. Gao, H. Li, and L.-P. Wang. Lattice boltzmann simulation of turbulent flow laden with finite-size particles. *Computers & Mathematics with Applications*, 2011.
- [19] J. O. Hinze. *Turbulence*. McGraw-Hill, 1975.
- [20] H. Homann and J. Bec. Finite-size effects in the dynamics of neutrally buoyant particles in turbulent flow. *Journal of Fluid Mechanics*, 651(1):81–91, 2010.
- [21] Brändlde de Motta Jorge César. *Simulation des écoulements turbulents avec des particules de taille finie en régime dense*. PhD thesis, Université de Toulouse, 2013.
- [22] I. Kataoka. Local instant formulation of two-phase flows. *Int. J. Multiphase Flow*, 12:745–758, 1986.
- [23] F. E. Kruis and K. A. Kusters. The collision rate of particles in turbulent flow. *Chemical Engineering Communications*, 158(1):201–230, 1997.
- [24] J. Lavieville. *Simulations numériques et modélisation des interactions entre l'entraînement par la turbulence et les collisions interparticulaires en écoulements gaz-solide*. PhD thesis, Université de Rouen, Rouen, March 1997.
- [25] D. Legendre, C. Daniel, and P. Guiraud. Experimental study of a drop bouncing on a wall in a liquid. *Physics of Fluids*, 17(9):097105–13, 2005.
- [26] F. Lucci, A. Ferrante, and S. Elghobashi. Modulation of isotropic turbulence by particles of taylor length-scale size. *Journal of Fluid Mechanics*, 650:5–55, 2010.
- [27] F. Lucci, A. Ferrante, and S. Elghobashi. Is stokes number an appropriate indicator for turbulence modulation by particles of taylor-length-scale size? *Physics of Fluids*, 23(2):025101, 2011.
- [28] N. N. Mansour and A. A. Wray. Decay of isotropic turbulence at low reynolds number. *Physics of Fluids*, 6:808, 1994.
- [29] A. Naso and A. Prosperetti. The interaction between a solid particle and a turbulent flow. *New Journal of Physics*, 12(3):033040, March 2010.
- [30] C. Poelma, J. Westerweel, and G. Ooms. Particle-fluid interactions in grid-generated turbulence. *Journal of Fluid Mechanics*, 589(-1):315–351, 2007.
- [31] N. M. Qureshi, U. Arrieta, C. Baudet, A. Cartellier, Y. Gagne, and M. Bourgoïn. Acceleration statistics of inertial particles in turbulent flow. *The European Physical Journal B*, 66(4):531–536, December 2008.
- [32] T.N. Randrianarivelo, G. Pianet, S. Vincent, and J.-P. Caltagirone. Numerical modelling of solid particle motion using a new penalty method. *Int. J. Numer. Meth. Fluids*, 47:1245–1251, 2005.
- [33] W. J. Rider and D. B. Kothe. Reconstructing volume tracking. *J. Comput. Phys.*, 141(2):112–152, April 1998.

- [34] J. B. Ritz and J. P. Caltagirone. A numerical continuous model for the hydrodynamics of fluid particle systems. *International Journal for Numerical Methods in Fluids*, 30(8):1067–1090, 1999.
- [35] C. Rosales and C. Meneveau. Linear forcing in numerical simulations of isotropic turbulence: Physical space implementations and convergence properties. *Physics of Fluids*, 17:095106, 2005.
- [36] P. G. Saffman and J. S. Turner. On the collision of drops in turbulent clouds. *Journal of Fluid Mechanics*, 1(01):16–30, 1956.
- [37] X. Shao, T. Wu, and Z. Yu. Fully resolved numerical simulation of particle-laden turbulent flow in a horizontal channel at a low reynolds number. *Journal of Fluid Mechanics*, pages 1–26, January 2012.
- [38] Kyle D. Squires and John K. Eaton. Particle response and turbulence modification in isotropic turbulence. *Physics of Fluids A: Fluid Dynamics*, 2(7):1191, 1990.
- [39] S. Sundaram and L.R. Collins. Collision statistics in an isotropic particle-laden turbulent suspension. part 1. direct numerical simulations. *Journal of Fluid Mechanics*, 335(75):109, 1997.
- [40] T. Tanaka and J. K. Eaton. Sub-kolmogorov resolution partical image velocimetry measurements of particle-laden forced turbulence. *Journal of Fluid Mechanics*, 643:177, January 2010.
- [41] C.M. Tchen. *Mean value and correlation problems connected with the motion of small particles suspended in a turbulent fluid*. PhD thesis, University of Delft, The Hague, 1947.
- [42] A. ten Cate, J. J. Derksen, L. M. Portela, and H. E. A. Van Den Akker. Fully resolved simulations of colliding monodisperse spheres in forced isotropic turbulence. *Journal of Fluid Mechanics*, 519:233–271, November 2004.
- [43] P. Trontin, S. Vincent, J. L. Estivalezes, and J. P. Caltagirone. Direct numerical simulation of a freely decaying turbulent interfacial-flow. *International Journal of Multiphase Flow*, 2010.
- [44] S. Vincent, J. C. Brändle de Motta, A. Sarthou, J.-L. Estivalezes, O. Simonin, and E. Climent. A lagrangian VOF tensorial penalty method for the DNS of resolved particle-laden flows. *Journal of Computational Physics*, 256:582–614, January 2014.
- [45] S. Vincent, A. Sarthou, J.-P. Caltagirone, F. Sonilhac, P. Février, C. Mignot, and G. Pianet. Augmented Lagrangian and penalty methods for the simulation of two-phase flows interacting with moving solids. Application to hydroplaning flows interacting with real tire tread patterns. *Journal of Computational Physics*, 230:956–983, 2011.
- [46] G. A. Voth, A. La Porta, A. M. Crawford, J. Alexander, and E. Bodenschatz. Measurement of particle accelerations in fully developed turbulence. *Journal of Fluid Mechanics*, 469, October 2002.
- [47] L.-P. Wang, O. Ayala, H. Gao, C. Andersen, and K. L. Mathews. Study of forced turbulence and its modulation by finite-size solid particles using the lattice boltzmann approach. *Computers & Mathematics with Applications*, 67(2):363–380, February 2014.
- [48] J.J.E. Williams and R.I. Crane. Particle collision rate in turbulent flow. *International Journal of Multiphase Flow*, 9(4):421 – 435, 1983.

- [49] A. M. Wood, W. Hwang, and J. K. Eaton. Preferential concentration of particles in homogeneous and isotropic turbulence. *International Journal of Multiphase Flow*, 31(10-11):1220–1230, 2005.
- [50] H. Xu and E. Bodenschatz. Motion of inertial particles with size larger than kolmogorov scale in turbulent flows. *Physica D: Nonlinear Phenomena*, 237(14-17):2095–2100, 2008.
- [51] W.-C. Yang. *Handbook of fluidization and fluid-particle systems*. CRC press, 2003.
- [52] Z. Zhang and A. Prosperetti. A second-order method for three-dimensional particle simulation. *Journal of Computational Physics*, 210(1):292–324, November 2005.